ELSEVIER

Biochimica et Biophysica Acta 1276 (1996) 106–116

BBA Biochimica et Biophysica Acta

Magnetic interaction between Q_A^- and the triplet state of the primary donor in modified reaction centers of the photosynthetic bacterium *Rhodobacter sphaeroides* R26

M.K. Bosch [a], P. Gast [a], E.M. Franken [a], G. Zwanenburg [b], P.J. Hore [b], A.J. Hoff [a,*]

[a] *Department of Biophysics, Huygens Laboratory, Leiden University, PO box 9504, 2300 RA Leiden, The Netherlands*
[b] *Physical and Theoretical Chemistry Laboratory, Oxford University, South Parks Road, Oxford, OX1 3QZ, UK*

Received 1 November 1995; revised 25 March 1996; accepted 17 April 1996

Abstract

The interaction between the reduced primary acceptor quinone (Q_A^-), and the triplet state of the primary donor ^3D is investigated with time-resolved continuous-wave EPR. The trough at high-field in the Q_A^- electron-spin polarized X-band EPR-spectrum at early delay times after the laser flash [De Groot et al. (1985) Biochim. Biophys. Acta 808, 13–20] is studied as a function of temperature and of the delay, in zinc-reconstituted reaction centers, with and without carotenoid. In all cases investigated a decrease in ^3D concentration is accompanied by a simultaneous attenuation of the high-field trough in the Q_A^- EPR spectrum. These observations confirm the hypothesis that the line-shape of Q_A^- at short delay times is influenced by a magnetic interaction with ^3D. The line-shape of the Q_A^- electron-spin polarized EPR spectrum directly after the laser flash, could be very well simulated using an extension of the model of Hore et al. [Hore, P.J. et al. (1993) Biochim. Biophys. Acta 1141, 221–230], with a dipolar coupling between Q_A^- and ^3D of -0.125 mT.

Keywords: Photosynthesis; Reaction center; Electron spin polarization; Quinone; Triplet; Iron removal; Carotenoid; Electron paramagnetic resonance; Spectral simulation

1. Introduction

Primary photochemistry in bacterial photosynthesis takes place in the photosynthetic reaction center (RC). The structure of the RC has been elucidated by X-ray analysis of the crystallized RC of several purple bacteria [1–4]. The cofactors are arranged in two chains with near C_2 symmetry. Electron transport, however, takes place along one direction, the so-called A-chain. After capture of a photon an excited singlet state of the primary donor (D^*) is formed. Subsequently an electron is released from D^* and transferred to the primary acceptor, a bacteriopheophytin molecule (Φ_A). Further electron transport results in reduction of the primary acceptor, a complex of a quinone molecule (Q_A) and a high-spin Fe^{2+} ($S = 2$) ion. If electron transport beyond Φ_A is blocked, for example because Q_A is reduced or chemically removed, then the spin-correlated primary radical pair $[D^{+\cdot}\Phi_A^{-\cdot}]$ can decay via different routes. Charge recombination takes place via the singlet decay channel to return the primary donor to its ground (D) or excited state (D^*), and via the triplet channel to give the molecular triplet state of the donor, ^3D [5]. In the RC of *Rhodobacter (Rb.) sphaeroides* R26 used in the present investigation, D is a bacteriochlorophyll *a* dimer, Φ_A a bacteriopheophytin *a* and Q_A a ubiquinone-10 molecule.

In RCs in which the reduced quinone is decoupled from the iron, the presence of dipolar and exchange interactions in the three-spin system $D^{+\cdot}\Phi_A^{-\cdot}Q_A^{-\cdot}$ produces a spin-polarized EPR signal of Q_A^- [6]. Because the shape of this spectrum depends strongly on the size, sign and anisotropy

Abbreviations: Car, carotenoid; D, primary donor; *DAF*, delay after a laser flash; EPR, electron paramagnetic resonance; ESP, electron spin polarization; RC, reaction center; Φ_A, primary acceptor; $\mathcal{T}(Q_A^-)$, trough in high-field wing of Q_A^- ESP spectrum.

* Corresponding author. Fax: +31 71 5275819; e-mail: Hoff@rulhl1.LeidenUniv.nl.

PII S0005-2728(96)00064-3

of these interactions, the study of electron spin polarization (ESP) spectra is one of the few ways to determine principal values, orientation and *sign* of the dipolar and exchange couplings between the primary reactants of photosynthesis. Recently, a model for the ESP of the $Q_A^{-\cdot}$ anion was presented by Hore et al. [7]. In contrast to earlier attempts to understand the Q-band (35 GHz) light-induced EPR spectrum of $Q_A^{-\cdot}$ in perdeuterated RCs of *Rhodospirillum rubrum* [8], in this model the three electron spins of $D^{+\cdot}$, $\Phi_A^{-\cdot}$ and $Q_A^{-\cdot}$ are treated as one system, coupled through dipolar and exchange interactions. The populations of the resulting eight-level system are calculated by a quantum-mechanical treatment of the spin dynamics. The anisotropic ESP observed in perdeuterated $Q_A^{-\cdot}$ was shown to arise from an interplay of the dipolar coupling between $Q_A^{-\cdot}$ and $\Phi_A^{-\cdot}$, the anisotropic g-tensor of $Q_A^{-\cdot}$ and the electronic exchange interaction between $\Phi_A^{-\cdot}$ and $D^{+\cdot}$. The main conclusion following from that work was that the exchange coupling between $D^{+\cdot}$ and $\Phi_A^{-\cdot}$ is positive in *Rhodospirillum rubrum*.

Some time ago, De Groot et al. [9] found additional structure in the emissively polarized EPR spectrum of $Q_A^{-\cdot}$. This structure consists mainly of a trough in the high-field wing (henceforth designated as $\mathcal{T}(Q_A^{-\cdot})$) and is only present at early (< 1 ms) delay times after an exciting laser flash (*DAF*). On the basis of its lifetime (~ 250 μs), it was suggested that $\mathcal{T}(Q_A^{-\cdot})$ was the result of a magnetic interaction between spin-polarized $Q_A^{-\cdot}$ and ^3D. This interaction was not included in the simulation of Hore et al. [7], because it was argued that the ^3D-concentration in the spectra detected under continuous illumination would be very low, and therefore could be neglected.

For a complete description of the polarization of $Q_A^{-\cdot}$, it is of interest to verify whether the additional structure $\mathcal{T}(Q_A^{-\cdot})$ can be simulated by the ESP model of Hore et al. [7]. Moreover, it is desirable to establish more firmly the role of the dipolar magnetic interactions amongst $D^{+\cdot}$, $\Phi_A^{-\cdot}$, $Q_A^{-\cdot}$ and ^3D in shaping $\mathcal{T}(Q_A^{-\cdot})$ and to determine accurately their numerical values. To this end, we have first investigated the electron spin polarization of $Q_A^{-\cdot}$ in two types of iron-depleted zinc-constituted RCs: (a) in RCs from the carotenoidless mutant *Rb. sphaeroides* R26 (Zn-RCs) and (b) in RCs from the same mutant, in which carotenoid (Car) had been reconstituted (Car Zn-RCs) [10]. In the latter RCs rapid triplet-triplet energy transfer from ^3D to ^3Car occurs at temperatures above 40 K [11,12]. We use the formation of ^3Car to change the concentration of ^3D, by varying the temperature at which the EPR spectra are measured. Thus, by studying the electron-spin polarization of $Q_A^{-\cdot}$ by time-resolved EPR as a function of temperature, the relation between the magnitude of $\mathcal{T}(Q_A^{-\cdot})$ and the EPR-amplitude of ^3D can be investigated. Secondly, we report on a simulation of the ESP spectrum of $Q_A^{-\cdot}$, directly after flash excitation, using an extension of the model of Hore et al. [7] that includes the dipolar interaction between $Q_A^{-\cdot}$ and ^3D.

2. Materials and methods

2.1. Preparation

RCs of *Rb. sphaeroides* 2.4.1 were isolated as in Ref. [13]. RCs of *Rb. sphaeroides* R26 were isolated from chromatophores as described in [14], or using a more rapid method described briefly as follows. Chromatophores ($OD_{860} = 50$ cm^{-1}) were incubated for 5 min with 5% (w/v) LDAO at room temperature, followed by a short centrifugation step to remove any debris. To this solution DEAE-Sephacel was added (about 25 g per 100 ml). After one minute the suspension was poured onto a glass filter and washed with 500 ml Tris/LDAO buffer (10 mM Tris, 0.025% (w/v) LDAO, 1 mM EDTA, pH 8). The dark blue effluent was discarded and the RCs were removed from the DEAE sephacel with 0.5 M NaCl in Tris/LDAO. Final purification and replacement of LDAO by Brij-58 was done with a DEAE sephacel column. After washing with 25 mM NaCl in a Tris-Brij buffer (10 mM Tris, 0.1% (w/v) Brij-58) the RCs were eluted from the column with a salt gradient (0.025–0.5 M NaCl). The absorption spectrum of these RCs was as in Ref. [14], except that the A_{280}/A_{802} ratio was a little higher (1.6), indicating somewhat more non-RC protein for the rapid preparations than reported for the standard preparation [14]. Our experimental results were not affected by this difference. Iron removal was achieved as in Ref. [15] and zinc reconstitution as in Ref. [16]. Spheroidene was extracted from *Rb. sphaeroides* 2.4.1 cells as in Refs. [17,18] and reconstituted into the RCs, after which the excess spheroidene was removed by washing on a DEAE column [10]. The optical spectrum of these Car Zn-RCs was as in Ref. [10], showing that the spheroidene was bound to the RC. Before transferring the RCs to the EPR tube, glycerol was added to 60–70% (v/v) to prevent cracking upon freezing. In all samples the quinone was photoreduced by freezing under illumination in the presence of sodium ascorbate.

2.2. Experimental procedures

Optical time-resolved experiments were performed with a home-built single-beam spectrophotometer [19]. The RCs were excited with a Q-switched Nd:YAG laser (15 ns flashes at 532 nm, 100 mJ per pulse). The time resolution of the spectrometer was determined by the pulse duration of the laser flashes.

X-band EPR measurements were performed on a Varian E9 X-band (9 GHz) EPR spectrometer equipped with an Oxford Instruments ESR900 flow cryostat. The lock-in detector of the instrument was modified to permit the recording of transient EPR signals with an instrumental rise time of 30 μs, using 100 kHz field modulation. All field-swept transient EPR spectra were recorded with field modulation using lock-in detection and a Princeton Applied Research model 162 Boxcar averager, equipped with

a model 165 gated integrator plug-in unit. The aperture duration was 10 μs. Boxcar-averaged spectra were recorded in AC mode, resulting in light-minus-dark spectra. To quantify the trough $\mathscr{T}(Q_A^{-\cdot})$, the spectrum at 1 ms (Fig. 4B) was subtracted from each of the polarized spectra recorded at earlier times, having first scaled the low-field part of the former to that of each of the latter. We define the amplitude of $\mathscr{T}(Q_A^{-\cdot})$ as the sum of the (absolute) heights with respect to the baseline of all peaks of the resulting four-peak difference spectrum (see inset Fig. 4B).

The RCs were excited with a Continuum NY61-10 Nd:YAG laser in series with a Continuum TS60 Titanium-Sapphire solid state laser, producing 10 ns light flashes at 852 nm with a power of ~ 10 mW. The repetition rate of the laser was 10 Hz. Data were collected on a personal computer. Data processing and simulations were done on a personal computer and also on a Sun SPARCstation 2.

2.3. Simulation of the $Q_A^{-\cdot}$ ESP spectrum

Fundamentally, the electron spin polarization in $Q_A^{-\cdot}$ arises because the dipolar coupling between $Q_A^{-\cdot}$ and $\Phi_A^{-\cdot}$ drives the singlet-triplet interconversion of the spin-correlated radical pair $[D^{+\cdot}\Phi_A^{-\cdot}]$. As argued qualitatively in [20] and quantitatively in [7], the efficiency of this process depends on the spin state of the unpaired electron on $Q_A^{-\cdot}$, α ($m_S = 1/2$) or β ($m_S = -1/2$), with the result that the populations of the *eight* electron spin states of $[D^{+\cdot}\Phi_A^{-\cdot}]Q_A^{-\cdot}$ become polarized. When $[D^{+\cdot}\Phi_A^{-\cdot}]$ undergoes charge recombination to give $^3DQ_A^{-\cdot}$ (with rate constant k_T) or $DQ_A^{-\cdot}$ (with rate constant k_S), these polarizations are carried over to the *six* spin states of the former (i.e., $T_{+1}\alpha$, $T_{+1}\beta$, $T_0\alpha$, $T_0\beta$, $T_{-1}\alpha$, $T_{-1}\beta$, where T_{+1}, T_0 and T_{-1} are the high-field Zeeman states of ^3D, and the α and β refer to $Q_A^{-\cdot}$ and the *two* spin states of the latter (i.e., $S\alpha$ and $S\beta$) as indicated schematically in Fig. 1A. There are thus four polarized contributions to the $Q_A^{-\cdot}$ EPR spectrum, corresponding to the three states of the primary donor triplet (T_{+1}, T_0, T_{-1}) together with the singlet (S) ground state of D.

The EPR spectrum of $Q_A^{-\cdot}$ was calculated as follows. For a particular orientation of the RC in the magnetic field ($\boldsymbol{B}_0$), the four $Q_A^{-\cdot}$ polarizations were computed using the approach of Hore et al. [7] in which the coherent evolution of $[D^{+\cdot}\Phi_A^{-\cdot}]Q_A^{-\cdot}$ under the influence of Zeeman, exchange and dipolar interactions, and the incoherent kinetics of charge recombination are modelled using a stochastic Liouville equation method. Full details of this calculation are given in Ref. [7]. The spectrum is constructed by building

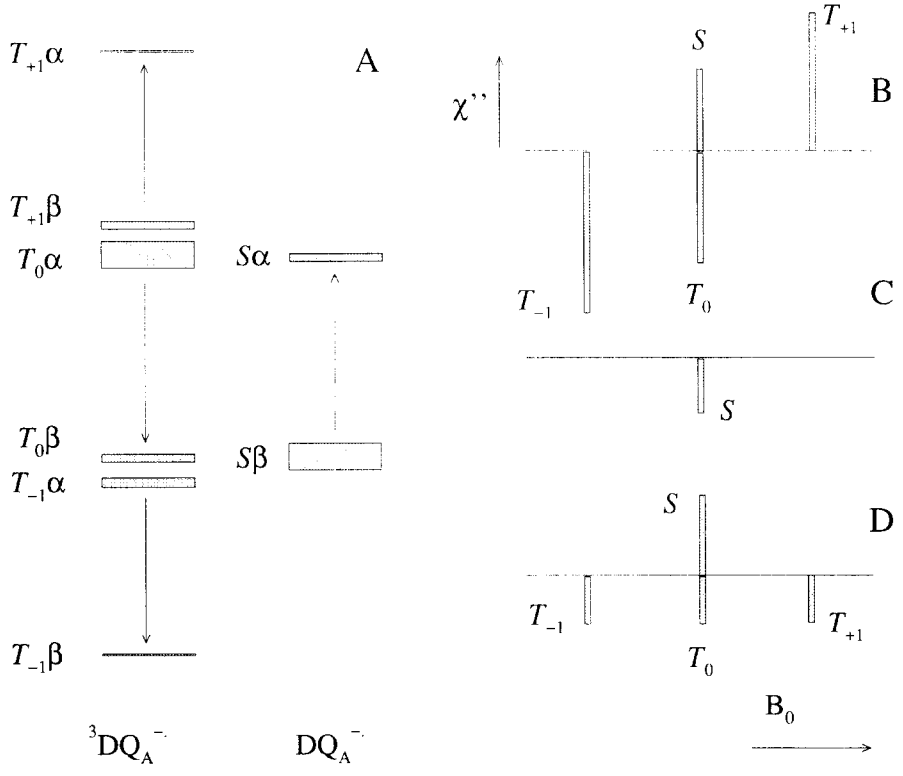

Fig. 1. A: Schematic energy levels of $Q_A^{-\cdot}$ in the presence of ^3D (left-hand side) and D (right-hand side), showing typical electron spin populations, whose magnitudes are indicated by the thickness of the horizontal bars [7]. The four $Q_A^{-\cdot}$ EPR transitions are shown by vertical arrows. B: Schematic EPR spectrum of $Q_A^{-\cdot}$ comprising the four components shown in A. The shift of the $T_{\pm 1}$ lines relative to the S and T_0 lines arises from the dipolar coupling of $Q_A^{-\cdot}$ to ^3D. C: Schematic EPR spectrum of $Q_A^{-\cdot}$ after ^3D has decayed. D: Schematic EPR spectrum of $Q_A^{-\cdot}$ following complete relaxation of the ESP in ^3D. These are the 'stick' spectra referred to in the text, prior to line broadening and orientational averaging. Sticks above the baseline are absorptive, those below the baseline are emissive.

'stick' spectra in which the heights of the sticks are given by the calculated polarizations, which may be positive or negative, and the positions of the sticks are determined by the effective g-value of $Q_A^{-\cdot}$ (g_{Q_A}) (the g-value for a particular orientation) together with the ^3D-$Q_A^{-\cdot}$ dipolar coupling. Specifically the four resonance frequencies were taken as:

$$\begin{aligned}
&\nu(S)Q_A^{-\cdot}: g_{Q_A}\mu_B B_0/\hbar,\\
&\nu(T_{+1})Q_A^{-\cdot}: g_{Q_A}\mu_B B_0/\hbar + 2D_{DQ_A}\left(\cos^2\gamma_{DQ_A} - 1/3\right),\\
&\nu(T_0)Q_A^{-\cdot}: g_{Q_A}\mu_B B_0/\hbar,\\
&\nu(T_{-1})Q_A^{-\cdot}: g_{Q_A}\mu_B B_0/\hbar - 2D_{DQ_A}\left(\cos^2\gamma_{DQ_A} - 1/3\right),
\end{aligned} \tag{1}$$

where D_{DQ_A} is the (axial) dipolar coupling parameter for $^3DQ_A^{-\cdot}$, and γ_{DQ_A} is the angle between the ^{3}D-$Q_A^{-\cdot}$ vector and the direction of the external magnetic field B_0. A schematic stick spectrum is shown in Fig. 1B. Note that the four components of the $Q_A^{-\cdot}$ spectrum are not degenerate: the $Q_A^{-\cdot}$ transitions in the presence of $^3D(T_{+1})$ and $^3D(T_{-1})$ are shifted by the dipolar coupling between ^3D and $Q_A^{-\cdot}$. The trough $\mathscr{T}(Q_A^{-\cdot})$ in the spin-polarized spectrum arises, indirectly, from these dipolar shifts, as shown below. As in Ref. [20], the stick spectra are then convolved with a Gaussian function to mimic the line-broadening effect of unresolved hyperfine couplings and spin relaxation, and then summed over a sphere, including the anisotropies of the Zeeman and dipolar interactions. This model bears a substantial similarity to the theory of EPR of correlated radical pairs [21].

Two modifications of this procedure were needed. First, to calculate the spectrum of $Q_A^{-\cdot}$ after ^3D had decayed, the calculation was repeated with $D_{DQ_A} = 0$. This leaves the polarizations unchanged (because they are generated in the $[D^{+\cdot}\Phi_A^{-\cdot}]Q_A^{-\cdot}$ state *before* $^3DQ_A^{-\cdot}$ is formed by charge recombination), but causes the three $^3DQ_A^{-\cdot}$ EPR transitions to collapse onto the $DQ_A^{-\cdot}$ line (because the dipolar coupling no longer exists). This is shown schematically in Fig. 1C in which the EPR signal has the *net* polarization of the four lines in Fig. 1B. Second, the polarized spectrum of $Q_A^{-\cdot}$, after the spin polarization of ^3D has fully relaxed, is obtained by replacing each of the three $^3DQ_A^{-\cdot}$ polarizations by their mean (i.e., the relatively small equilibrium polarization is ignored). As shown in Fig. 1D, the EPR intensity of $DQ_A^{-\cdot}$ is unchanged, and the $Q_A^{-\cdot}$ polarization in the presence of ^3D is now independent of the spin state of ^3D.

To include anisotropic hyperfine couplings, in an approximate fashion, an axial line-broadening aligned with the y-axis of the $Q_A^{-\cdot}$ g-tensor (the vector in the plane of the quinone ring perpendicular to the carbonyl bonds) was added to the isotropic broadening mentioned above. The choice of the y-axis is suggested by the W-band EPR spectrum of $Q_A^{-\cdot}$ recorded by Burghaus et al. [22].

In each case, difference spectra were obtained by subtracting from the simulated 'light' spectrum described above, a 'dark' spectrum calculated assuming equilibrium polarizations and no ^{3}D-$Q_A^{-\cdot}$ coupling.

3. Results

3.1. Time-resolved optical measurements

In reduced wild-type RCs of *Rb. sphaeroides* 2.4.1 and Car Zn-RCs the build-up and decay of the carotenoid triplet state was monitored with optical laser flash spectroscopy. ^{3}Car kinetics were detected at 547.5 nm. The kinetic traces were fitted to the function [23]

$$[^3\mathrm{Car}](t) = \frac{k_1[^3\mathrm{D}]_0}{k_2 - k_1}\left(\mathrm{e}^{-k_1 t} - \mathrm{e}^{-k_2 t}\right), \tag{2}$$

with $[^3D]_0$ the concentration of ^3D from which triplet-triplet energy transfer to ^{3}Car takes place, $k_1 = 1/\tau_{rise}$ and $k_2 = 1/\tau_{decay}$. The temperature dependence of the kinetic parameters obtained from the fit is depicted in Fig. 2. Both RC preparations show ^{3}Car formation at temperatures higher than 40 K (Fig. 2A1, 2B1). At 50 K the rise-time (τ_{rise}) of the triplet has a maximum, at $\sim$ 600 ns (Fig. 2A2, 2B2); at 20 K it is instrument-limited ($\sim$ 15 ns). The two RC preparations differ with respect to the decay time (τ_{decay}), which diminishes monotonically from 70 μs at 10 K, to 8 μs at 87 K in Car Zn-RCs (Fig. 2A3). In wild-type RCs τ_{decay} diminishes monotonically from 35 μs at 10 K to 8 μs at 100 K (Fig. 2B3). Thus, at low temperature τ_{decay} is a factor of two faster in wild-type RCs as compared to the carotenoid Zn-RCs, whereas at high temperature it is about equal for both preparations.

3.2. Triplet EPR of D and Car

In reduced Car Zn-RCs of *Rb. sphaeroides* R26 the EPR spectrum of ^3D with the characteristic polarization pattern AEE AAE (A: enhanced absorption; E: emission) [24] and $|D| = 188 \times 10^{-4}\mathrm{cm}^{-1}$, $|E| = 32 \times 10^{-4}\mathrm{cm}^{-1}$ [25], was observed at 4 K in a light-modulation experiment. When the temperature was raised to 40 K, mainly ^{3}Car with reversed polarization pattern EAA EEA and $|D| = 286 \times 10^{-4}\mathrm{cm}^{-1}$, $|E| = 44 \times 10^{-4}\mathrm{cm}^{-1}$ was observed, as reported earlier by Chadwick et al. [11] (data not shown). From this observation, and from the optical measurements, we conclude that our spheroidene reconstitution was successful and leads to active RCs in which triplet-triplet energy transfer from ^3D to ^{3}Car at 40 K takes place, as in native RCs.

Time-resolved EPR field-swept spectra were taken at $DAF = 50$ μs in reduced Zn-RCs and Car Zn-RCs as a function of temperature (Fig. 3). Fig. 3A shows the spectra for Zn-RCs. Raising the temperature results in a decrease

of this triplet signal, mainly due to increased spin-lattice relaxation [12]. This faster T_1 reduces the large ESP in ^{3}D within the 50 μs delay between light excitation and EPR-detection. Fig. 3C shows similar experiments done with Car Zn-RCs. Already at 20 K some ^{3}Car has formed as indicated by the two outermost peaks in the spectrum. At 40 K and 60 K only ^{3}Car was observed.

3.3. Electron spin polarization of Q_A^-

In all samples in the dark the familiar near-Gaussian cw-EPR signal of Q_A^- was observed. Under continuous illumination this signal becomes emissively polarized while shifting slightly to lower magnetic field [6] (data not shown).

Fig. 4B shows the time-resolved ESP spectra of Q_A^- in Zn-RCs, obtained at 20 K for different *DAF*. At short *DAF* the signal shows the high-field trough $\mathcal{T}(Q_A^-)$ in the field-swept spectrum. At later times, $\mathcal{T}(Q_A^-)$ decreases in amplitude, and at *DAF* = 1 ms it has disappeared completely. These observations are in accordance with the measurements of De Groot et al., who used RCs in which the iron was magnetically uncoupled from Q_A^-, and probably removed [9]. At the same *DAF* values, the spectrum of ^{3}D was recorded (Fig. 4A). At *DAF* = 50 μs a strong ^{3}D signal is observed. The intensity of the ^{3}D signal is smaller at longer *DAF*. Fig. 5A clearly shows that the amplitudes of the EPR signal of ^{3}D (recorded at $\boldsymbol{B}_0 \| Z$) and of $\mathcal{T}(Q_A^-)$ are correlated.

The temperature dependence of $\mathcal{T}(Q_A^-)$ in Zn-RCs at *DAF* = 50 μs is shown in Fig. 3B. These spectra were recorded at relatively low microwave power (30 μW) in order to reduce microwave-induced relaxation and to eliminate contributions of ^{3}D; the straight baseline at low and high magnetic field indicates that ^{3}D contributions can indeed be neglected in these spectra. $\mathcal{T}(Q_A^-)$ is observed at all temperatures between 20 K and 80 K, becoming less intense with increasing temperature. At the same *DAF* values, the ^{3}D spectrum was recorded (Fig. 3A). The gradual decrease of $\mathcal{T}(Q_A^-)$ as the temperature is increased is accompanied by a corresponding decrease of the ^{3}D signal (see Fig. 5B open circles, and Fig. 4).

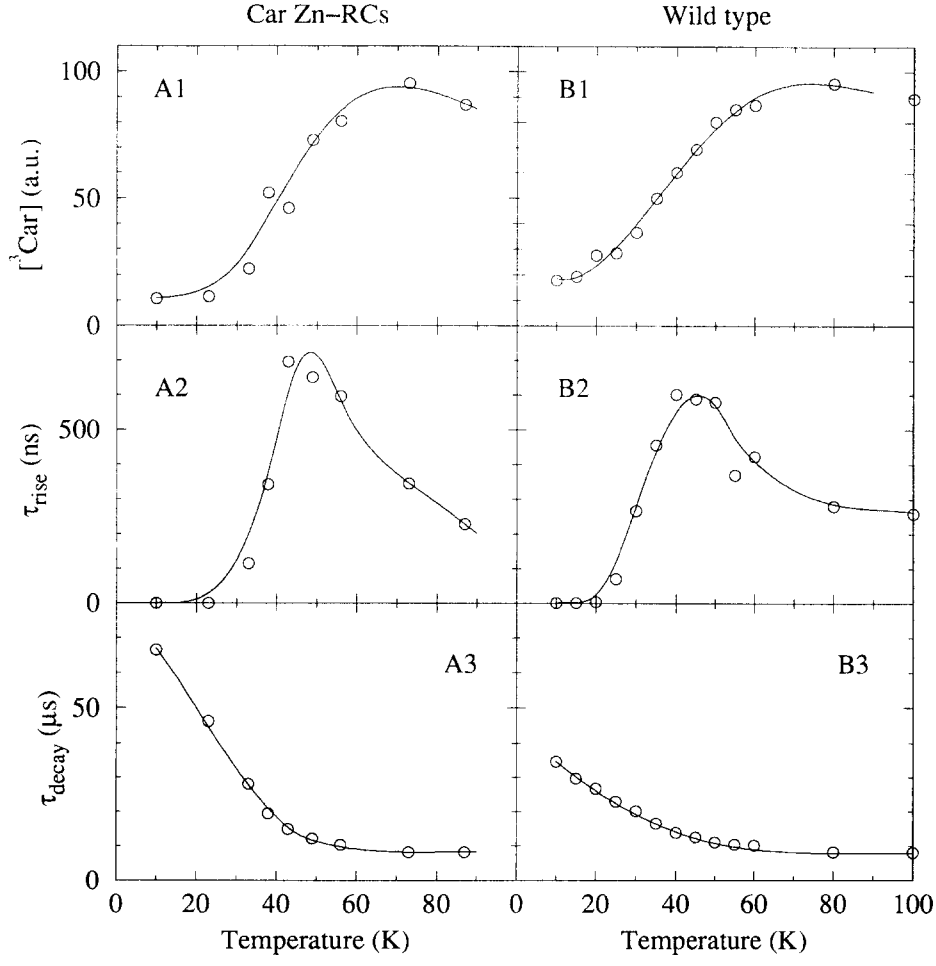

Fig. 2. Temperature dependence of kinetic parameters of ^{3}Car in (A) carotenoid reconstituted *Rb. sphaeroides* R26 and (B) in wild-type RCs, obtained by fitting the optical kinetics with Eq. 2. Panel 1 shows the amplitude, panel 2 the risetime τ_{rise}, and panel 3 the decay time τ_{decay} of the carotenoid triplet state. Lines are guides to the eye. Experimental conditions: Exciting laser flash 100 mJ at 532 nm, pulse length 15 ns; detection wavelength 547.5 nm.

Fig. 3D shows the temperature dependence of the $Q_A^{-\cdot}$ signal at $DAF = 50$ μs for Car Zn-RCs. At 20 K, $\mathcal{T}(Q_A^{-\cdot})$ is observable, though its amplitude is much smaller than that observed in Zn-RCs. Above 40 K, however, $\mathcal{T}(Q_A^{-\cdot})$ rapidly disappears with increasing temperature. Concomitant with the disappearance of $\mathcal{T}(Q_A^{-\cdot})$ the ^{3}D signal ceases to be observable, and instead the broad carotenoid triplet signal is observed (Fig. 3C). The temperature dependence of $\mathcal{T}(Q_A^{-\cdot})$ in Car Zn-RCs is depicted in Fig. 5B.

3.4. Simulation of the $Q_A^{-\cdot}$ spectrum

To simulate the polarized $Q_A^{-\cdot}$ ESP spectra in the presence of ^{3}D, the model used by Hore et al. for the 35 GHz EPR spectrum of deuterated $Q_A^{-\cdot}$ [7] was extended, as outlined in Section 2. The initial values of the various parameters involved were taken from Ref. [7], except for the principal g-tensor components of $D^{+\cdot}$ and $Q_A^{-\cdot}$, for which more recent and more accurate measurements were used [22,26] (see Table 1). The $D^{+\cdot}Q_A^{-\cdot}$ dipolar coupling ($D_{DQ_A} = -0.125$ mT) was calculated from X-ray coordinates using a point dipole approximation.

Initial attempts to reproduce the polarized spectrum, using an isotropic line-broadening ΔB_{iso}, failed. For no combination of the rate constants k_S and k_T ΔB_{iso} could the trough $\mathcal{T}(Q_A^{-\cdot})$ satisfactorily be simulated. Prompted by recent W-band EPR studies of semiquinone anions in model systems [22], an axial anisotropic component was added to the broadening, such that the linewidth became

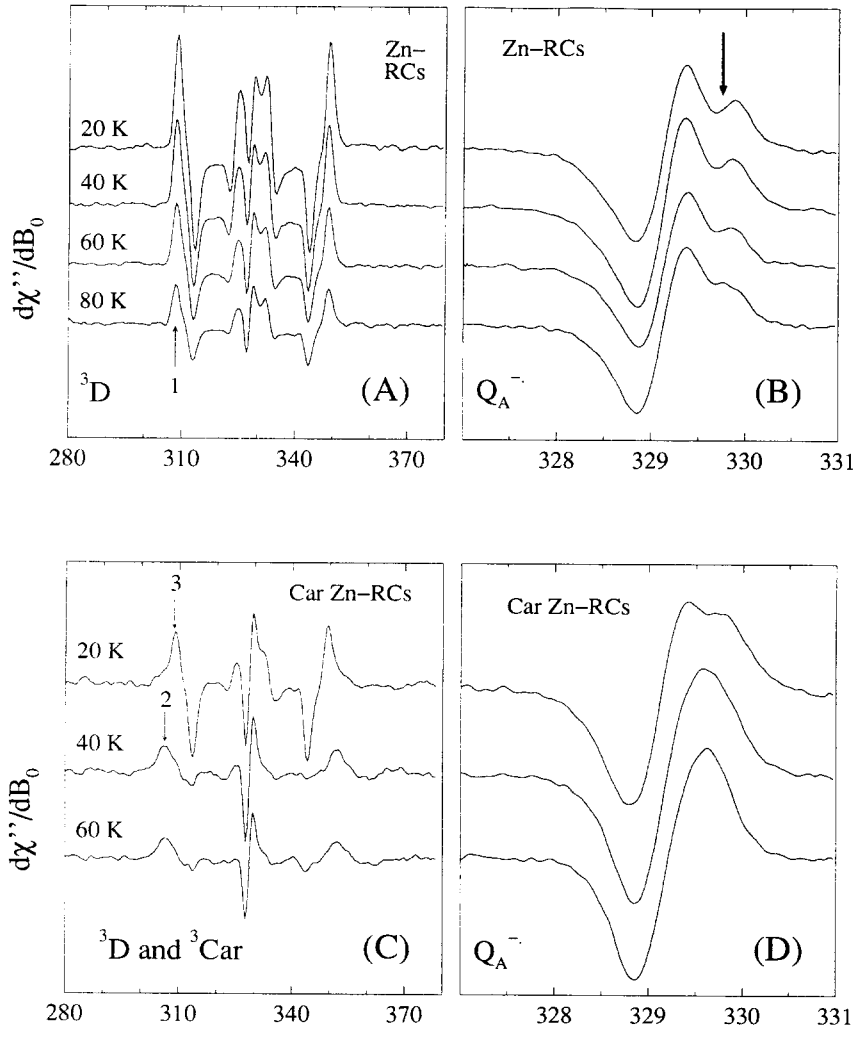

Fig. 3. Temperature dependence of ^{3}D, ^{3}Car and $Q_A^{-\cdot}$ EPR signals in Zn-RCs and in Car Zn-RCs, detected at $DAF = 50$ μs. Panels (A) and (C) show EPR spectra of ^{3}D and ^{3}Car, respectively. The central line is due to $Q_A^{-\cdot}$ and is enlarged in panels (B) and (D). The arrow in panel (B) indicates the trough $\mathcal{T}(Q_A^{-\cdot})$. Experimental conditions: exciting laser flash: 10 mJ at 852 nm, pulse length 10 ns; 10 μs boxcar gate; microwave frequency: 9.203 GHz; microwave power: 10 mW (triplet spectra) or 30 μW ($Q_A^{-\cdot}$ spectra); magnetic field modulation: 2 mT (triplet spectra), 0.2 mT ($Q_A^{-\cdot}$ spectra).

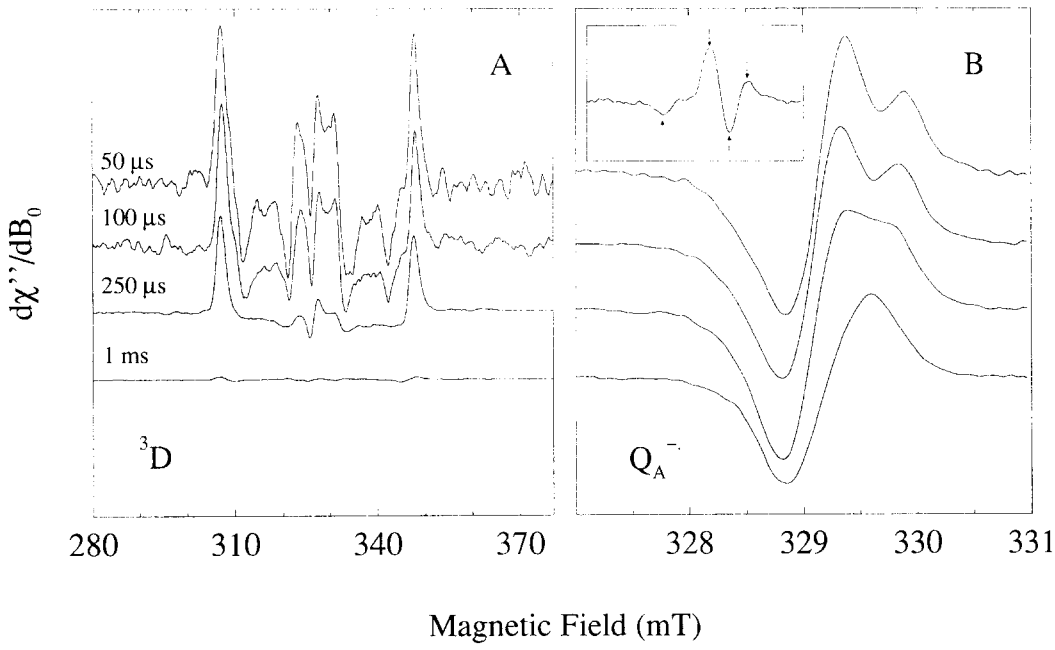

Fig. 4. Time dependence of ^{3}D (panel A) and Q_A^- (panel B) EPR spectra in Zn-RCs. Spectra are recorded at the indicated *DAF*. $T = 20$ K; other experimental conditions as in Fig. 3. The inset shows the four-peak difference spectrum for $DAF = 50$ µs, obtained as indicated in Section 2. Arrows indicate the peaks used for quantification of $\mathcal{T}(Q_A^-)$. The magnetic field scale is the same as for the other Q_A^- spectra.

$\Delta B_{iso} + \Delta B_{aniso}(\cos^2\theta - 1/3)$, in which θ is the angle between the applied field direction and a specified axis in Q_A^-. Extensive searches of the k_S,k_T, ΔB_{iso}, ΔB_{aniso} parameter space, maintaining all other quantities as in Table 1, showed that the trough $\mathcal{T}(Q_A^-)$ could not be simulated when the axis of the anisotropy coincided with the x-axis of Q_A^- (running through the carbonyl oxygens), or the z-axis (perpendicular to the plane of the quinone ring), but *was* obtained using the y-axis. Fig. 6 shows the most convincing simulation of the 50 µs spectrum of Zn RCs, corresponding to $k_s = 2.1 \times 10^7\ s^{-1}$, $k_T = 7.8 \times 10^8\ s^{-1}$, $\Delta B_{iso} = 0.56$ mT, $\Delta B_{aniso} = 0.35$ mT. No other, significantly different, set of values reproduced as satisfactorily the depth and width of $\mathcal{T}(Q_A^-)$ and the relative amplitudes and positions of the other extrema in the spectrum. Indeed, the simulated spectra are rather sensitive to k_S and k_T (see Fig. 7), making this an attractive method for obtaining the magnitudes of these rate constants.

The parameters used for Fig. 6 gave a dark spectrum with the correct shape (approximately Gaussian) and a width at half maximum height of 0.9 mT, compared to the observed width of 1.0 mT. Note that the fully relaxed dark spectrum is independent of k_S and k_T and depends only on the principal g-values of Q_A^-, and the two linewidth parameters. The minor discrepancy in linewidth should not be seen as a serious shortcoming of the model. It has a

Table 1
Parameters used for the simulation of the ESP spectrum of Q_A^- in interaction with ^{3}D

$g_{xx,D}$	2.00329	g_{xx,Q_A}	2.0067	$g_{x,D}$	0.854	−0.249	−0.457
$g_{yy,D}$	2.00239	g_{yy,Q_A}	2.0054	$g_{y,D}$	0.303	−0.477	0.825
$g_{zz,D}$	2.00203	g_{zz,Q_A}	2.0024	$g_{z,D}$	−0.423	−0.843	−0.332
g_{Φ_A}	2.0036						
				g_{x,Q_A}	0.148	−0.923	−0.356
$J_{D\Phi_A}$	0.5 mT	$D_{D\Phi_A}$	−0.48 mT	g_{y,Q_A}	0.041	0.356	−0.934
$J_{\Phi_AQ_A}$	0.18 mT	$D_{\Phi_AQ_A}$	−1.2 mT	g_{z,Q_A}	0.988	0.153	0.014
J_{DQ_A}	0 mT	D_{DQ_A}	−0.125 mT				
				dipolar axes			
k_S	$2.1 \times 10^7 s^{-1}$	ΔB_{iso}	0.56 mT	$D\Phi_A$	−0.625	−0.704	0.337
k_T	$7.8 \times 10^8 s^{-1}$	ΔB_{aniso}	0.35 mT	Φ_AQ_A	0.208	−0.698	0.685
				DQ_A	−0.302	−0.784	0.542

$g_{ii,D}$ and g_{ii,Q_A} ($i = x,y,z$) are the principal g-values of D^+ and Q_A^-; g_{Φ_A} is the (isotropic) g-value of Φ_A^-; $J_{D\Phi_A}$, $J_{\Phi_AQ_A}$, J_{DQ_A} and $D_{D\Phi_A}$, $D_{\Phi_AQ_A}$, D_{DQ_A} are exchange (J) and dipolar (D) couplings between the indicated co-factors. ΔB_{iso} and ΔB_{aniso} are the isotropic and anisotropic line broadenings of Q_A^-. At the right-hand side the three numbers represent the cosine of the angle between the specified axis and, respectively, the crystallographic x, y, z axis. These cosines are obtained from the X-ray structure [4]; for g_D we used orientation I from Refs. [27,36].

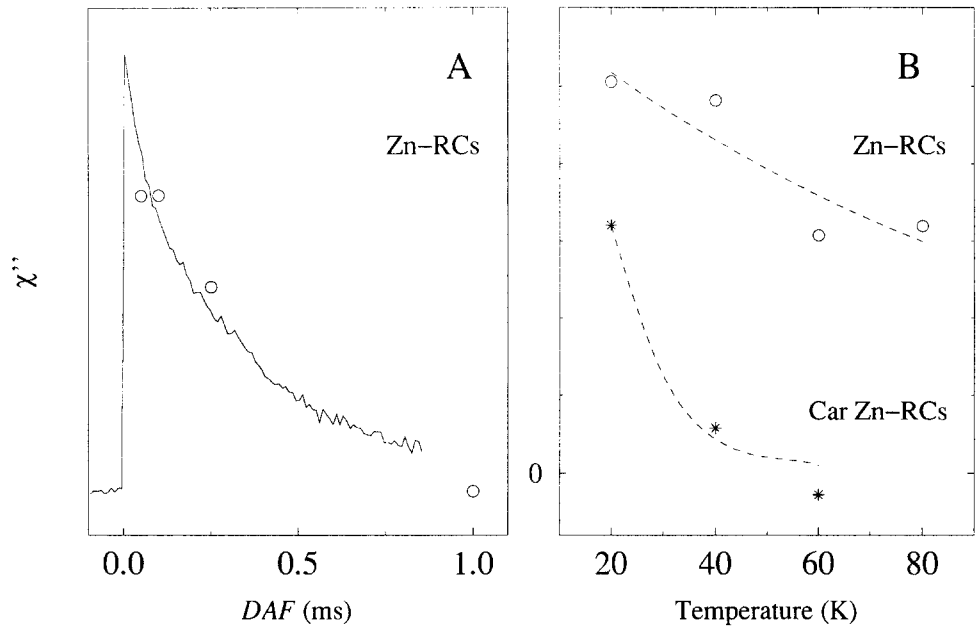

Fig. 5. Comparison of the amplitude of $\mathcal{T}(Q_A^-)$ and the ^3D decay (measured at $B_0||Z$) (panel A) and the temperature dependence of $\mathcal{T}(Q_A^-)$ in Zn-RCs and in Car Zn-RCs (panel B). The amplitude of $\mathcal{T}(Q_A^-)$ was determined as indicated in Section 2. The line in panel A represents the triplet decay; symbols indicate the amplitude of $\mathcal{T}(Q_A^-)$ for Zn-RCs (○) and Car Zn-RCs (∗). Dashed lines in panel B are guides to the eye.

precedent in the radical pair $D^{+\cdot}Q_A^{-\cdot}$ in Zn^{2+}-substituted RCs, whose polarized X-band EPR spectra typically require a line-broadening of ~0.65 mT [27], which also gives simulated dark spectra of width 0.9 mT. The origin of this difference is not known, but may be related to the very different line-shapes predicted and observed for tran-

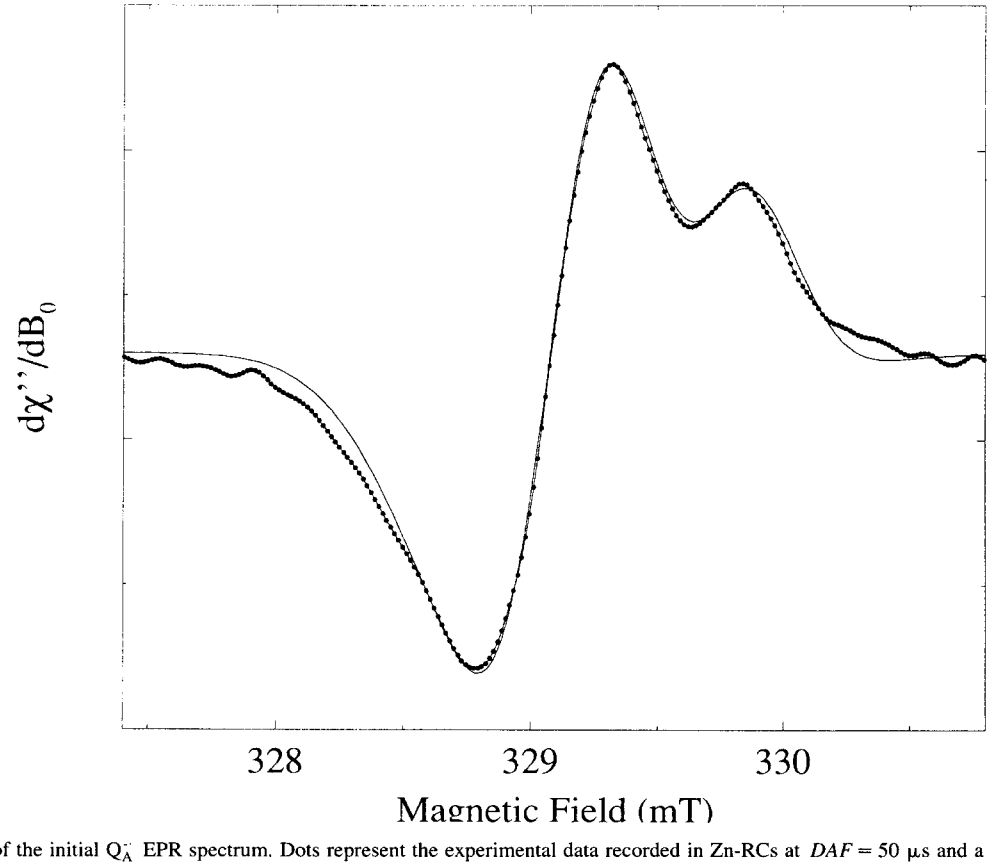

Fig. 6. Simulation of the initial Q_A^- EPR spectrum. Dots represent the experimental data recorded in Zn-RCs at $DAF = 50$ μs and a temperature of 20 K; other experimental conditions as in Fig. 3. The line is the EPR spectrum calculated with the parameters shown in Table 1.

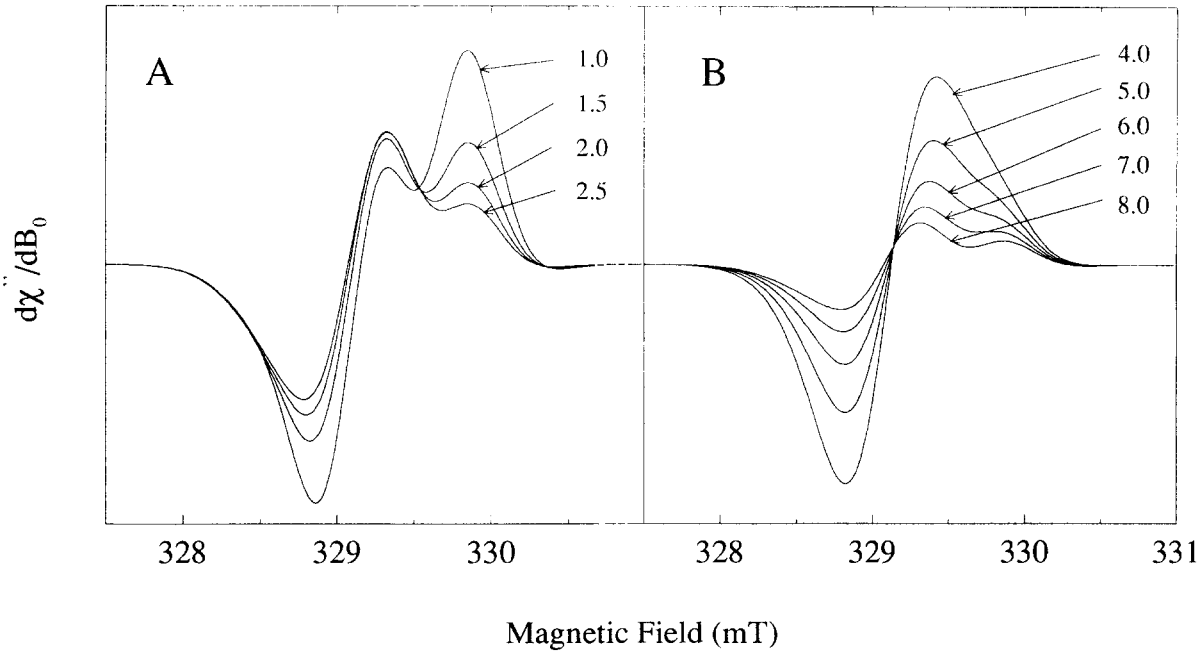

Fig. 7. Simulated EPR spectra of $Q_A^{\cdot-}$ showing the dependence on the rate constants k_S (A) and k_T (B). Rate constants are indicated in the figure ($\times 10^{-7}$ s^{-1}). All other parameters as in Table 1.

sient nutation spectra at short and long delays after the creation of the radicals observed [28].

A spin-polarized spectrum was also calculated using the parameters in Table 1, but with D_{DQ_A} changed from -0.125 mT to zero to investigate the effect of the disappearance of ^{3}D. Fig. 8 shows the resulting spectra for the two values of D_{DQ_A}, including the four components referred to in Fig. 1. As found experimentally, the $D_{DQ_A} = 0$ spectrum (Fig. 8B) has no trough. The origin of $\mathscr{T}(Q_A^{\cdot-})$ is seen to arise subtly from the partial cancellation of the positive and negative parts of the four sub-spectra. The small shifts in the T_{+1} and T_{-1} components, Eq. (2), when D_{DQ_A} vanishes are sufficient to abolish the effect. It is also evident from Fig. 8 why the calculated spectra are so sensitive to k_S and k_T: small changes in the shapes and/or amplitudes of the sub-spectra can be expected to

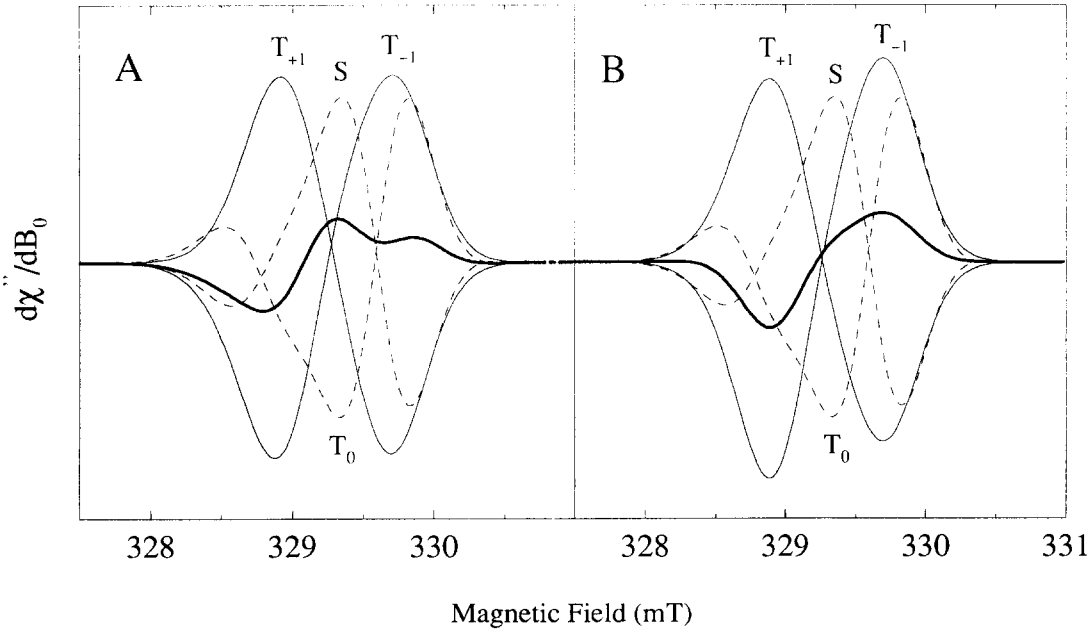

Fig. 8. Simulated EPR spectra of $Q_A^{\cdot-}$ showing the four constituent sub-spectra. (A) $D_{DQ_A} = -0.125$ mT. (B) $D_{DQ_A} = 0.0$ mT. All other parameters as in Table 1.

have a large influence on their sum. A similar principle has been used to account for the sensitivity of the polarized spectrum of $D^{+\cdot}$ to the g-tensor of the iron-quinone complex $[Q_A^{-\cdot}Fe^{2+}]$ in native bacterial reaction centers [29]. Finally, a simulation of the spectrum of $Q_A^{-\cdot}$ in the presence of fully relaxed ^3D (not shown) is also devoid of a trough, in agreement with the experimental observation.

4. Discussion

The changes in the EPR-spectrum of $Q_A^{-\cdot}$ at early *DAF*, previously observed by De Groot et al. [9] in iron-decoupled material of *Rb. sphaeroides* 2.4.1 [30] at 20 K, are shown also to be present in Zn-RCs of *Rb. sphaeroides* R26 (Fig. 4A). Thus, we may conclude that, at 20 K, the presence of the short-lived $\mathscr{T}(Q_A^{-\cdot})$ is observed in all reduced RC preparations in which the primary quinone is magnetically uncoupled from the non-heme iron.

In the present work we unambiguously demonstrate that there is a one-to-one relation between the presence of $\mathscr{T}(Q_A^{-\cdot})$ and the concentration of ^3D, constituting conclusive evidence that $\mathscr{T}(Q_A^{-\cdot})$ is caused by a magnetic interaction between ^3D and $Q_A^{-\cdot}$.

The $Q_A^{-\cdot}$ ESP spectrum is very well simulated by our extension of the model of Hore et al. [7] using reasonable values for the parameters. The simulations show that the trough $\mathscr{T}(Q_A^{-\cdot})$ disappears if $D_{DQ_A} = 0$, or if the triplet sublevels of ^3D are in Boltzmann equilibrium, which is consistent with our experimental observations, and reinforces the assignment of $\mathscr{T}(Q_A^{-\cdot})$ to a magnetic interaction between $Q_A^{-\cdot}$ and ^3D that is dipolar in nature. The value of D_{DQ_A} used in the simulations is that calculated from the X-ray structure. The value of k_S found ($2.1 \times 10^7\ s^{-1}$) is, within experimental error, the same as that found by Ogrodnik et al. ($(1.5 \pm 0.6) \times 10^7 s^{-1}$) [31]. Several values of k_T have been determined from static magnetic field effects [32,33], RYDMR spectroscopy [34,35] and the spin-polarized EPR spectrum of $Q_A^{-\cdot}$ [7]. The value found here ($7.8 \times 10^8\ s^{-1}$) is within the error limits identical to the mostrecent value for k_T at low temperature ($(8.4 \pm 1) \times 10^8 s^{-1}$ [33]).

5. Conclusions

From the time and temperature dependence of $\mathscr{T}(Q_A^{-\cdot})$ (the additional structure at high field in the spin-polarized EPR spectrum of $Q_A^{-\cdot}$), and of the ^3D signal in Zn-RCs with and without reconstituted carotenoid, we have unambiguously demonstrated that $\mathscr{T}(Q_A^{-\cdot})$ is a manifestation of a magnetic interaction between $Q_A^{-\cdot}$ and ^3D.

The experimental spectrum at early times after the laser flash could be simulated very well, using the dynamic model of anisotropic electron spin polarization of Hore et al. [7], extended with a dipolar interaction between ^3D and $Q_A^{-\cdot}$. The simulation is consistent with a dipolar coupling of -0.125 mT between ^3D and $Q_A^{-\cdot}$, calculated from the X-ray structure assuming point dipoles. The successful simulation confirms the model of Hore et al. for ESP of $Q_A^{-\cdot}$ produced by the three-spin complex $D^{+\cdot}\Phi_A^{-\cdot}Q_A^{-\cdot}$ [7], and therefore indirectly their conclusion that the exchange interaction between $D^{+\cdot}$ and $\Phi_A^{-\cdot}$ is positive.

Acknowledgements

The authors would like to thank I.I. Proskuryakov and J.S. van den Brink for assistance during the measurements. We are grateful to Ms. S.J. Jansen, who isolated the reaction centers. This work was supported by the Netherlands Foundation for Chemical research (SON), financed by the Netherlands Organization for Scientific Research (NWO). M.K.B. and G.Z. are grateful to the European Commission (Grant number SC1* CT090-0569) for travel grants and a postdoctoral fellowship, respectively. P.G. is a research fellow of the Royal Netherlands Academy of Arts and Sciences (KNAW).

References

[1] Deisenhofer, J., Epp, O., Miki, K., Huber, R. and Michel, H. (1985) Nature 318, 618–624.
[2] Allen, J.P., Feher, G., Yeates, T.O., Komiya, H. and Rees, D.C. (1987) Proc. Natl. Acad. Sci. USA 84, 5730–5734.
[3] Komiya, H., Yeates, T.O., Rees, D.C., Allen, J.P. and Feher, G. (1988) Proc. Natl. Acad. Sci. USA 85, 9012–9016.
[4] Ermler, U., Fritzsch, G., Buchanan, S.K. and Michel, H. (1994) Structure 2, 925–936.
[5] Parson, W.W., Clayton, R.K. and Cogdell, R.J. (1975) Biochim. Biophys. Acta 387, 265–278.
[6] Gast, P. and Hoff, A.J. (1979) Biochim. Biophys. Acta 548, 520–535.
[7] Hore, P.J., Riley, D.J., Semlyen, J.J., Zwanenburg, G. and Hoff, A.J. (1993) Biochim. Biophys. Acta 1141, 221–230.
[8] Gast, P., de Groot, A. and Hoff, A.J. (1983) Biochim. Biophys. Acta 723, 52–58.
[9] De Groot, A., Lous, E.J. and Hoff, A.J. (1985) Biochim. Biophys. Acta 808, 13–20.
[10] Agalidis, I., Lutz, M. and Reiss-Husson, F. (1980) Biochim. Biophys. Acta 589, 264–274.
[11] Chadwick, B.W. and Frank, H.A. (1986) Biochim. Biophys. Acta 851, 257–266.
[12] Hoff, A.J. and Proskuryakov, I.I. (1985) Chem. Phys. Lett. 115, 303–310.
[13] Shochat, S., Arlt, T., Francke, C., Gast, P., Van Noort, P.I., Otte, S.C.M., Schelvis, H.P.M., Schmidt, S., Vijgenboom, E., Vrieze, J., Zinth, W. and Hoff, A.J. (1994) Photosynth. Res. 40, 55–66.
[14] Feher, G. and Okamura, M.Y. (1978) in The Photosynthetic Bacteria (Clayton, R.K. and Sistrom, W.R., eds.) pp. 349–386, Plenum Press, New York.
[15] Tiede, D.M. and Dutton, P.L. (1981) Biochim. Biophys. Acta 637, 278–290.
[16] Debus, R.J., Feher, G. and Okamura, M.Y. (1986) Biochemistry 25, 2276–2287.
[17] Goodwin, T.W., Land, D.G. and Osman, H.G. (1955) Biochem. J. 59, 491–496.
[18] Schneour, E.A. (1962) Biochim. Biophys. Acta 62, 534–540.

[19] Smit, H.W.J., Amesz, J. and Van der Hoeven, M.F.R. (1987) Biochim. Biophys. Acta 893, 232–240.
[20] Hore, P.J., Hunter, D.A., Riley, D.J., Semlyen, J.J., Van Wijk, F.G.H., Schaafsma, T.J., Gast, P. and Hoff, A.J. (1991) Res. Chem. Interm. 16, 127–139.
[21] Hore, P.J. (1989) in Advanced EPR. Applications in Biology and Biochemistry (Hoff, A.J., ed.) pp. 405–440, Elsevier, Amsterdam.
[22] Burghaus, O., Plato, M., Rohrer, M., Möbius, K., MacMillan, F. and Lubitz, W. (1993) J. Phys. Chem. 97, 7639–7647.
[23] Alberty, R.A. (1983) Physical Chemistry, pp. 612–613, Wiley, New York, 6th edition.
[24] Dutton, P.L., Leigh, J.S. and Seibert, M. (1972) Biochem. Biophys. Res. Commun. 46, 406–413.
[25] Den Blanken, H.J., Van der Zwet, G.P. and Hoff, A.J. (1982) Chem. Phys. Lett. 85, 335–338.
[26] Burghaus, O., Plato, M., Bumann, D., Neumann, B., Lubitz, W. and Möbius, K. (1991) Chem. Phys. Lett. 185, 381–386.
[27] Van den Brink, J.S., Hulsebosch, R.J., Gast, P., Hore, P.J. and Hoff, A.J. (1994) Biochemistry 33, 13668–13677.
[28] Hore, P.J., McLauchlan, K.A., Frydkjaer, S. and Muus, L.T. (1981) Chem. Phys. Lett. 77, 127–130.
[29] Van den Brink, J.S., Hermolle, T.E.P., Gast, P., Hore, P.J. and Hoff, A.J. (1996) J. Phys. Chem. 100, 2430–2437.
[30] Slooten, L. (1972) Biochim. Biophys. Acta 256, 452–466.
[31] Ogrodnik, A., Volk, M. and Michel-Beyerle, M.E. (1988) in The Photosynthetic Bacterial Reaction Centre (Breton, J. and Vermeglio, A., eds.) pp. 177–183, Plenum, New York.
[32] Ogrodnik, A., Remy-Richter, N., Michel-Beyerle, M.E. and Feick, R. (1987) Chem. Phys. Lett. 135, 576–581.
[33] Volk, M., Ogrodnik, A. and Michel-Beyerle, M.-E. (1995) in Anoxygenic Photosynthetic Bacteria (Blankenship, R.E., Madigan, M.T. and Bauer, C.D., eds.) pp. 595–626, Kluwer, Dordrecht.
[34] Norris, J.R., Bowman, M.K., Budil, D.E., Tang, J., Wraight, C.A. and Closs, G.L. (1982) Proc. Natl. Acad. Sci. USA 79, 5532–5536.
[35] Lersch, W. and Michel-Beyerle, M.E. (1989) in Advanced EPR. Applications in Biology and Biochemistry (Hoff, A.J., ed.) pp. 685–705, Elsevier, Amsterdam.
[36] Klette, R., Torring, J.T., Plato, M., Möbius, K., Bonigk, B. and Lubitz, W. (1993) J. Phys. Chem. 97, 2015–2020.